Two Synthesis Techniques Applied to Flutter Suppression on a Flight Research Wing

Irving Abel,* Boyd Perry III,† and Harold N. Murrow‡
NASA Langley Research Center, Hampton, Va.

This paper describes some activities associated with the preliminary design of an active control system for flutter suppression capable of demonstrating a 20% increase in flutter velocity. Results from two control system synthesis techniques are given. One technique uses classical control theory, and the other uses an "aerodynamic energy method," where control surface rates or displacements are minimized. Analytical methods used to synthesize the control systems and evaluate their performance are described. Some aspects of a program for flight testing the active control system are also given. This program, Drones for Aerodynamics and Structural Testing (DAST), employs modified drone-type vehicles for flight assessments and validation testing.

Nomenclature

$A(k)$ = generalized aerodynamic force
a_1, a_2 = control law gains used in energy method
b = reference semichord used in aerodynamic theory
c = chord length along centerline of control surface
b_r = semichord length along centerline of control surface, $c/2$
$D(s)$ = denominator polynomial in s
g = units of gravitational acceleration
h = vertical displacement at 30% of wing chord c
h_r = vertical displacement at fuselage reference point
k = reduced frequency, $\omega b/V$
k_m = aerodynamic lag
M = Mach number
$N(s)$ = numerator polynomial in s
s = Laplace variable
V = flight velocity
y = sensor output
y^* = fraction of wing semispan, measured from fuselage centerline
α = angle of attack of wing at wing chord c
α_r = angle of attack of fuselage at fuselage reference point
δ = control surface displacement
ρ = atmospheric density
ω = circular frequency
ζ = damping coefficient

Matrices

$[A_j], [D_j]$ = real aerodynamic matrix coefficients
$\{A_{j_\delta}\}, \{D_{j_\delta}\}$ = real aerodynamic matrix coefficients for control surfaces
$\{B\}$ = control surface input matrix
$[F_j]$ = real coefficients of equations of motion
$\lfloor G \rfloor$ = see Eq. (6)
$[I]$ = identity matrix
$[K]$ = generalized stiffness
$[M]$ = generalized mass
$\{M_\delta\}$ = mass unbalance of control surface
$\lfloor T(s) \rfloor$ = transfer function relating control surface response to wing motion
$\{q\}$ = generalized displacement vector
$[U]$ = matrix representing first-order equations of motion
$\{X\}$ = response vector of first-order equations of motion
$\begin{Bmatrix} Z_1 \\ Z_2 \end{Bmatrix}$ = displacement at sensor locations
$[\phi]$ = matrix of modal coefficients at sensor locations
$\dot{\ }\dot{\ }\dot{\ }$ = dot superscripts, indicate time derivatives

Presented as Paper 77-1062 at the AIAA 1977 Guidance and Control Conference, Hollywood, Fla., Aug. 8-10, 1977; submitted Sept. 10, 1977; revision received Feb. 1, 1978.

Index categories: Aeroelasticity and Hydroelasticity; Guidance and Control; Structural Dynamics.

*Aerospace Engineer, Dynamic Loads Branch.
†Aerospace Engineer, Dynamic Loads Branch. Member AIAA.
‡Aerospace Engineer, Dynamic Loads Branch. Associate Fellow AIAA.

Introduction

OVER the last several years considerable interst has emerged in applying active control technology to suppress aeroelastic response of present and future aircraft.[1-3] Application of this technology offers potential gains in aerodynamic efficiency and weight savings by providing ride quality control, gust and maneuver load control, flutter suppression, and by allowing for relaxed static stability. Through cooperative interdisciplinary efforts, especially among control specialists and aeroelasticians, a new class of aircraft may evolve in which active control systems are integrated into the initial vehicle design, and structural integrity is dependent on the adequate operation of an active control system.

A considerable amount of effort has been spent in advancing these concepts through analytical and wind tunnel studies.[4-6] A NASA flight program has subsequently been initiated to study active control concepts using remotely piloted vehicles. This program, Drones for Aerodynamic and Structural Testing (DAST), is a joint Langley Research Center and Dryden Flight Research Center program. The objectives of this program are to: 1) demonstrate active control concepts; 2) validate active control system performance; and 3) measure flight loads. The drone test technique is used to acquire free-flight data at conditions similar, except for Reynolds number, to those encountered in full-scale flight tests at reduced risk, cost, and time.

The purpose of this paper is to report on two preliminary synthesis studies of an active flutter suppression system to be tested on the first of several research wings in the DAST program. Results from applying both classical control theory, for example, Ref. 7, and an aerodynamic energy method[5,8,9]

are presented for design of an active flutter suppression system capable of providing a 20% minimum increase in flutter velocity for symmetric motion in a design gust environment. Control law synthesis techniques for both systems are described, along with the subsequent placement of controls, sensors, and simplified block diagrams. The following results provide insight into alternate approaches for accomplishing flutter suppression which may be useful for future applications. Also included is a general description of the flight vehicle and the mathematical models used to synthesize and evaluate control system performance.

Research Wing

Design

A research wing was designed with the unique feature that flutter will occur within the flight envelope of the vehicle-research wing combination. This wing is presently being fabricated and instrumented; a photograph of the wing is presented in Fig. 1. The cross-section view in Fig. 1 indicates the type of construction. Bending stiffness is primarily provided by the two steel spars positioned at 25% and 60% of the local chord. Torsional stiffness is primarily provided by the matrix of the fiberglass skins which are attached to the spars to form the wing box. By orienting the fibers along and normal to the wing elastic axis, the torsional stiffness is low enough to allow flutter within the flight envelope. As shown on the sketch, both leading and trailing edge wing sections are removable to provide access to instrumentation and active control system equipment installed in the wing.

An added feature of the wing (not shown) is the inclusion of small masses (0.90 kg) attached near the tip to allow for adjustment of the flutter boundary. These masses project aft of the trailing edge and are releasable. In case of flutter suppression system failure, an accelerometer acting as a g switch triggers their release, after which the wing is calculated to be flutter-free in the range of flight conditions where tests are to be conducted.

A three-view drawing of a Firebee II or BQM-34F flight vehicle-research wing combination to be used in the DAST program is shown in Fig. 2. The drone has been modified to improve controllability and research data acquisition. Flight tests will involve air launches from beneath the wing of a B-52 and midair recovery by helicopter after parachute deployment and will be conducted using remote piloted research vehicle (RPRV) facilities.

Flutter Analysis

For the purpose of these studies, the effects of fuselage flexibility are neglected. Therefore, as a basis for flutter analyses, a finite element NASTRAN model of the wing and carry-through structure is developed, the total fuselage mass is included but fuselage flexibility is neglected. A total of 127 nodes is used to model the front and rear spars, wing skins, ribs, leading and trailing edges, and center carry-through structure. Two rigid body modes and seven symmetric elastic modes are defined for analysis purposes. The seven elastic modes cover a frequency range of 9.9-128 Hz. Modes, frequencies, and generalized masses from the NASTRAN model are used in an aeroelastic analysis to define the wing flutter boundary.

Unsteady aerodynamic forces on the wing and horizontal tail are generated using doublet lattice aerodynamics by a numerical method similar to that described in Ref. 10. The unsteady aerodynamic pressure distributions are calculated by subdividing each lifting surface into an array of streamwise trapezoidal boxes with 121 boxes used to model the wing and 14 boxes used to model the horizontal tail. The lifting surface is then represented by a lattice of doublets along the ¼ chord of each box. The downwash boundary condition is satisfied at the ¾ chord of each box by equating the aerodynamic downwash to the slope and deflection of each structural mode.

Equations of Motion

The flutter equations are formulated in terms of real matrices by using an "approximating function" for the aerodynamic forces. This procedure is similar to that described in Ref. 11. The variation of the aerodynamic forces with reduced frequency is approximated by a rational polynomial in the Laplace variable, s. The pqth aerodynamic term is written

$$A_{pq}(k) \approx A_{0_{pq}} + A_{1_{pq}}\left(\frac{b}{V}\right)s + A_{2_{pq}}\left(\frac{b}{V}\right)^2 s^2 + \sum_{m=1}^{4}\left(D_{m_{pq}}s\right)\Big/\left(s+\frac{V}{b}k_m\right) \tag{1}$$

where p,q refers to the pth row and qth column, respectively. As described in Ref. 11, the form of Eq. (1) permits an approximation of the time delays inherent in unsteady aerodynamics, subject to the requirements of complex conjugate symmetry, denominator roots in the left-half plane, and a good approximation of the complex aerodynamic forces at $s=i\omega$. The approximating coefficients (A_0, A_1, A_2, $D_1 \ldots D_4$) in Eq. (1) are evaluated by a least-squares fit through values of complex aerodynamic terms at ten discrete reduced frequencies, $k=\omega b/V$. The values of k_m are arbitrarily selected from the range of reduced frequencies.

By using the approximating coefficients, the equations of motion, in terms of real matrices, are

$$\left[s^2[M]+[K]\right]\{q\} + \tfrac{1}{2}\rho V^2\left[s^2\left(\frac{b}{V}\right)^2[A_2] + s\left(\frac{b}{V}\right)[A_1] + [A_0] + \sum_{m=1}^{4}\frac{[D_m]s}{\left(s+\frac{V}{b}k_m\right)}\right]\{q\} = 0 \tag{2}$$

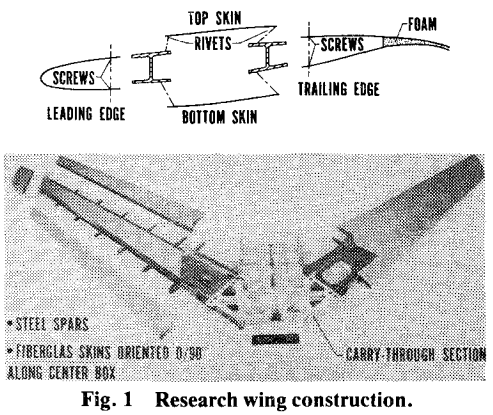

Fig. 1 Research wing construction.

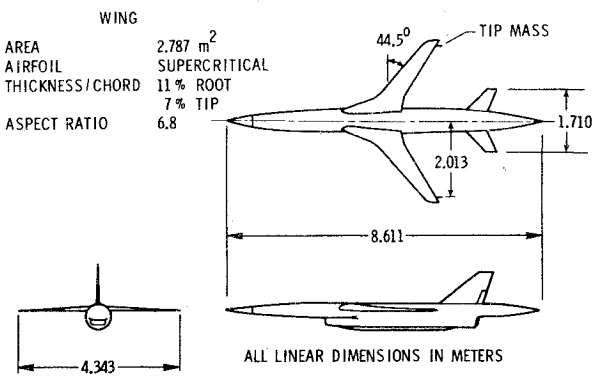

Fig. 2 Three-view drawing of research vehicle configuration.

where, for the present application, the matrices are 9×9 including two rigid body modes plus seven elastic modes. Multiplying through by the denominator terms yields a matrix polynomial in s of the form

$$([F_0]+[F_1]s+[F_2]s^2+\ldots+[F_n]s^n)\{q\}=0$$

where the matrix coefficients F_j are functions of Mach number, dynamic pressure, and velocity. The order of the resulting systems, n, is 6 for the present application. This equation can be reduced to the following series of 54 first-order equations:

$$s\{X\}=[U]\{X\} \tag{3}$$

where

$$\{X\}=\begin{Bmatrix} s^{n-1}\{q\} \\ s^{n-2}\{q\} \\ \vdots \\ s\{q\} \\ s^0\{q\} \end{Bmatrix}$$

and

$$[U]=\begin{bmatrix} [-F_n^{-1}F_{n-1}] & [-F_n^{-1}F_{n-2}] & \ldots & [-F_n^{-1}F_0] \\ [I] & 0 & & 0 \\ 0 & [I] & \ldots & 0 \\ \vdots & & & \vdots \\ 0 & 0 & \ldots[I] & 0 \end{bmatrix} \tag{4}$$

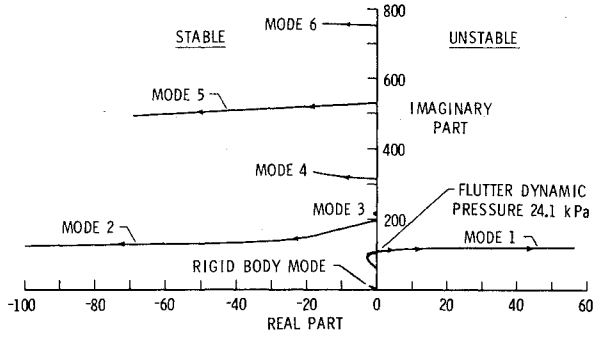

Fig. 3 Root locus at $M=0.9$ and altitude = 6750 m for basic wing.

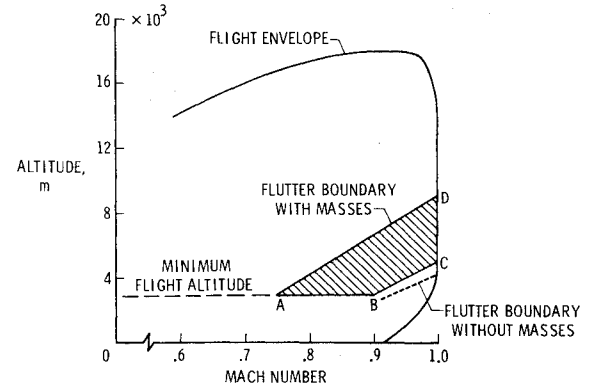

Fig. 4 Flight envelope, including region for operation of flutter suppression system.

The matrix $[U]$ is $9n\times9n$. For a fixed value of Mach number, velocity, and dynamic pressure, the eigenvalues of Eq. (4) are the roots of the characteristic flutter equation. Since the matrix elements F_j are functions of dynamic pressure, a root locus of the eigenvalues as a function of dynamic pressure can be constructed. These loci correspond to the variation in the roots as altitude is varied at a constant Mach number.

Results

A typical root locus calculated at $M=0.9$ and altitude at about 6750 m is shown in Fig. 3. This is the altitude for which the speed of sound is selected. Each curve that intersects the vertical axis corresponds to a structural degree of freedom (except the rigid body mode at $\omega=0$). A classical flutter behavior is apparent from Fig. 3, since the frequencies of modes one and two coalesce, with increasing dynamic pressure, as mode 1 crosses into the unstable region. A rapid degradation in damping coupled with the relatively high-flutter frequency suggests that the basic wing flutter is violent. Calculations performed at $M=0.8$ and 0.7 (not shown) indicate similar behavior.

The results of these calculations are presented in Fig. 4. The line $\overline{AD}$ represents the wing with tip masses, referred to hereafter as "basic wing" flutter boundary. The flutter boundary is not shown below 3050 m, since this altitude has been set as the minimum permissible flight altitude. The flutter dynamic pressures and frequencies for $M=0.9$, 0.8, and 0.7 are presented in columns 3 and 4 of Table 1. The dashed line in Fig. 4 indicates the flutter boundary for the wing without tip masses.

Flutter Suppression System Synthesis

Background

The design objective of the flutter suppression system is to provide a 20% increase in flutter speed above that of the basic wing. This increase is to be demonstrated in flight, except where limited by the flight envelope of the vehicle. The region for flight demonstration is shown in Fig. 4 by the shaded area $\overline{ABCD}$. The 20% increase is to be demonstrated along line $\overline{BC}$. Prior to final design and fabrication of hardware for the flutter suppression system, preliminary design studies were conducted. A contractual study[7] was an in-depth investigation using classical control law synthesis and included preliminary hardware specifications, hydraulic requirements, definition of electronic components, actuator hinge moment requirements, and recommendations for flight telemetry. An in-house study applied the aerodynamic energy method of control law synthesis.[5]

Closed-Loop Equations

The closed-loop equations of motion are presented for a single trailing-edge control; however, additional control surfaces can be included if necessary. The control laws derived for either the classical or the aerodynamic energy method can be cast into the general form hereafter described. A control law that relates control surface motion to the measured response is assumed to be of the form

$$\delta(s)=\lfloor T(s)\rfloor\begin{Bmatrix} Z_1 \\ Z_2 \end{Bmatrix} \tag{5}$$

where

$$\begin{Bmatrix} Z_1 \\ Z_2 \end{Bmatrix}=[\phi]\{q\} \quad \text{and} \quad \lfloor T(s)\rfloor=\frac{N(s)}{D(s)}\lfloor G\rfloor$$

Therefore,

$$\delta(s)=\frac{N(s)}{D(s)}\lfloor G\rfloor[\phi]\{q\} \tag{6}$$

By using the same aerodynamic approximating coefficients as presented in Eq. (1), the equations of motion with active controls can be written as

$$\left[s^2[M]+[K]\right]\{q\}+\tfrac{1}{2}\rho V^2\left[s^2\left(\frac{b}{V}\right)^2[A_2]+s\left(\frac{b}{V}\right)[A_1]+[A_0]+\sum_{m=1}^{4}\frac{[D_m]s}{\left(s+\frac{V}{b}k_m\right)}\right]\{q\}+\tfrac{1}{2}\rho V^2\left[s^2\left(\left(\frac{b}{V}\right)^2\{A_{2_\delta}\}+\frac{2}{\rho V^2}\{M_\delta\}\right)+s\left(\frac{b}{V}\right)\{A_{1_\delta}\}+\{A_{0_\delta}\}+\sum_{m=1}^{4}\frac{\{D_{m_\delta}\}s}{\left(s+\frac{V}{b}k_m\right)}\right]\frac{N(s)}{D(s)}\lfloor G\rfloor[\phi]\{q\}=0 \tag{7}$$

For the purpose of preliminary design, actuator dynamics and structural damping are not included. Compensating filters can be added to account for the actuator dynamics. However, control surface mass unbalance is included as the term $\{M_\delta\}$. In a manner similar to that described earlier, Eq. (7) can be reduced to a first-order system of equations of the form

$$s\{X\}=[U]\{X\}$$

The eigenvalues of $[U]$ are the roots of the closed-loop system.

Classical Control System Synthesis

Approach

As indicated in Ref. 7, the control system synthesis began with a parametric investigation to establish what combination of control surface locations and sensor locations would control the flutter mode and not adversely affect other vehicle modes. For this purpose, a zero locus is used to estimate modal coupling as a function of control surface and sensor location. Many combinations of these locations were eliminated either because of adverse coupling with other vehicle modes or because coupling with the flutter mode was small. A typical example, for two different control surface locations combined with three possible sensor locations along the rear spar, is given in Fig. 5. These results are determined by writing the open-loop equations of motion as

$$\{\dot{X}(s)\}=[U]\{X\}+\{B\}\delta$$

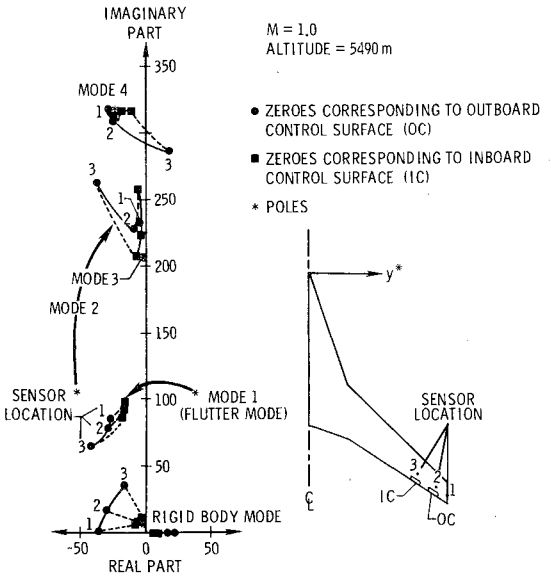

Fig. 5 Zero locus for vertical acceleration.

where B is a polynomial in s whose coefficients are functions of A_{j_δ}, D_{j_δ}, ρ, V, and k_m. This equation can also be written as

$$\{X(s)\}=[sI-U]^{-1}\{B\}\delta$$

Writing the output at the sensor as

$$y=\lfloor\phi\rfloor\{X\}$$

the transfer function y/δ can be written as

$$\frac{y}{\delta}=\frac{\lfloor\phi\rfloor[sI-U]^{\text{Adj}}\{B\}}{|sI-U|} \tag{8}$$

The numerator determines the zeroes of the system, while the denominator determines the poles of the system. The roots of the denominator of Eq. (8) are the same as the eigenvalues of Eq. (4).

As shown in Fig. 5, the outboard control surface moves the zeroes associated with the flutter mode farthest into the left-half plane indicating more potential for flutter mode damping. The arrows indicate movement of roots from poles to zeroes in modes 1 and 2. The poles and zeroes for mode 3 are coincident. Sensor location 3 ($y^*=0.79$) provides the best coupling with the flutter mode, but at the same time exhibits adverse coupling with mode 4. Sensor location 2 ($y^*=0.924$) was selected from this type of analysis, since it provides damping in the flutter mode and decouples mode 4 by placing the zero near the pole. Results presented in Fig. 5 are for control surfaces of 5.8% semispan, 20% chord, and with centerlines at $y^*=0.90$ and 0.78, respectively.

At this point, a gain root locus of direct acceleration feedback without compensation indicated that approximately 90 deg of phase lag is required to damp the flutter mode. A shaping filter was then designed to provide the 90 deg phase-lag requirements using a combination of methods including gain root loci, trial and error, and previous experience with similar systems.

The control synthesis procedure continued with an evaluation of the response of the control surfaces due to atmospheric turbulence along the boundary ABCD (Fig. 4). The control surface design constraints are for operation in a vertical gust environment defined by the von Kármán spectrum with a 3.66 m/s rms gust intensity and a scale length of 762 m. For the outboard control surface described previously, rms amplitudes were beyond the capability of the control surface actuator. The actuator described in Ref. 7 is capable of maximum rate and deflection of approximately 1020 deg/s, and ±12 deg, respectively. The control surface size was then doubled to 11.6% semispan. Due to this increased surface size, the shaping filter had to be modified to account for adverse coupling in the fifth structural mode and a second sensor located at $y^*=0.129$ was added to improve adverse coupling with the rigid body modes.

Closed-Loop Control Law

As a result of the synthesis study described in the previous section, the following control law was developed

$$\delta(s)=\frac{1158s}{(s+15)^2(s+80)}\left(\ddot{Z}_{y^*=0.924}-\ddot{Z}_{y^*=0.129}\right)$$

where $\ddot{Z}$ is in units of acceleration g measured at $y^*=0.924$ and 0.129, respectively. This form of the transfer function can be expressed in terms of Eq. (6) by letting

$N(s)$ = $1158s^3$, since $s\ddot{Z}=s^3Z$
$D(s)$ = $(s+15)^2(s+80)$
$\lfloor G\rfloor$ = $\lfloor 1-1\rfloor$
$[\phi]$ = matrix of modal coefficients at sensor locations

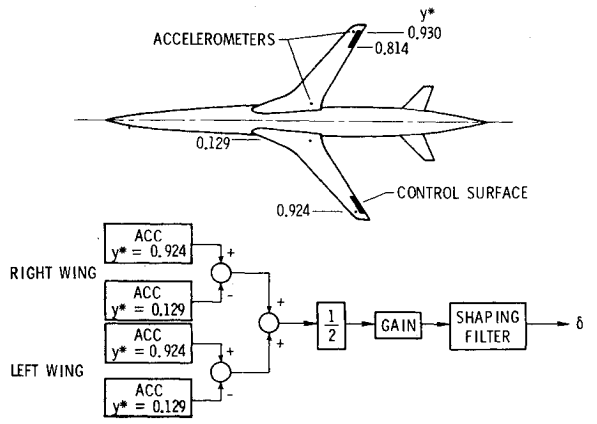

Fig. 6 Synthesized active control system – classical method.

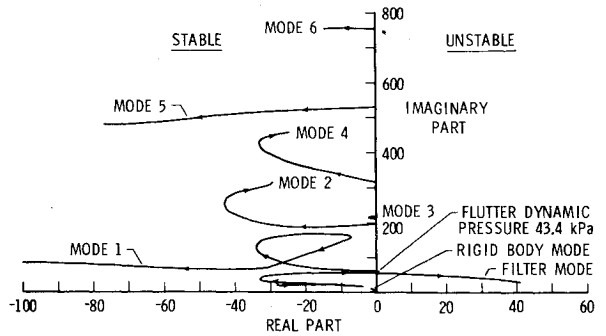

Fig. 7 Closed-loop root locus at $M=0.9$ and altitude = 2286 m (classical method).

The matrix $\lfloor G \rfloor$ provides for differencing the output at the sensor locations. A plan view of the vehicle indicating control surface locations, sensor locations, and a simplified block diagram of the feedback path of the closed-loop system is presented in Fig. 6.

System Performance

Figure 7 presents a typical closed-loop root locus (Eq. 7) calculated at $M=0.9$ and altitude = 2286m. Due to the change in the speed of sound with altitude, the results shown for the closed-loop cases are not for a matched flutter point. However, the differences in flutter dynamic pressure are not appreciable. Comparing these results with the no-control case in Fig. 3, an increase in flutter dynamic pressure of approximately 80% is indicated. It appears, from Fig. 7, that the flutter is delayed by decoupling the responses in flexible modes one and two. A closed-loop flutter point at a dynamic pressure of 43.4 kPa results from a coupling between the first structural mode and the filter mode introduced by the closed-loop transfer function. However, this crossing occurs beyond the required 20% increase in flutter velocity. Calculations at $M=0.8$ and 0.7 indicate a slightly different behavior, with the second flexible mode going unstable, but once again at a dynamic pressure well above the required flutter velocity. The closed-loop flutter dynamic pressures and frequencies for $M=0.9$, 0.8, and 0.7 are presented in Table 1. A gust response calculation indicates control surface rates and displacements within the system capability. For the Mach numbers investigated, maximum control surface activity occurs at $M=0.9$ and at an altitude of 3050 m.

Aerodynamic Energy Control System Synthesis

Approach

The aerodynamic energy method[5] was originally formulated in an attempt to provide active control system designs that are insensitive to changing flight conditions. Specific application of this method to flutter suppression[4] yielded encouraging results, but also indicated that the form of the control law could be improved. As a result of recent studies, a relaxed energy method has been formulated and reported in Ref. 8.

The relaxed energy method does not require the use of both leading and trailing edge control as proposed in Ref. 5. It does, however, allow "free parameters" to be introduced which enable the general form of the control law to be tailored to a specific application. These free parameters also permit the use of optimization procedures to minimize control surface activity during design. The control law used here is referred to in Ref. 8 as a localized damping-type transfer function. For this application, the constant term is deleted. For a single trailing edge control, this control law can be expressed as

$$\delta(s) = \left(\frac{a_1 s^2}{s^2 + 2\zeta_1\omega_1 s + \omega_1^2} + \frac{a_2 s^2}{s^2 + 2\zeta_2\omega_2 s + \omega_2^2} \right) \times \lfloor 4 \quad 2.8 \rfloor \begin{Bmatrix} Z_1 \\ Z_2 \end{Bmatrix}$$

To avoid coupling with the rigid body degrees of freedom, an extended version of the control law[9] is used. That is,

$$\begin{Bmatrix} Z_1 \\ Z_2 \end{Bmatrix} = \begin{Bmatrix} \dfrac{h - h_r}{b_r} \\ \\ \alpha - \alpha_r \end{Bmatrix}$$

where h, h_r, α, and α_r are measured at the locations indicated in Fig. 8. This form of the control law allows relative values of deflection and angle of attack to be input to the control law, thereby decoupling the rigid body from the flexible modes. This form of the transfer function can be expressed in terms of Eq. (6) by letting

$$\frac{N(s)}{D(s)} = \frac{a_1 s^2}{s^2 + 2\zeta_1\omega_1 s + \omega_1^2} + \frac{a_2 s^2}{s^2 + 2\zeta_2\omega_2 s + \omega_2^2} \qquad (9)$$

Table 1 Summary of calculated flutter characteristics

	Basic wing (no control)			Closed-loop					
				Classical			Energy		
Mach number	Alt., m	Dyn. press., kPa	Freq., Hz	Alt., m	Dyn. press., kPa	Freq., Hz	Alt., m	Dyn. press., kPa	Freq., Hz
0.9	6750	24.1	16.9	2286	43.4	8.6	1676	46.9	8.3
0.8	4350	26.2	18.0	–	NF[a]	–	–	NF[a]	–
0.7	1850	27.7	19.4	–	NF[a]	–	–	NF[a]	–

[a] No flutter to sea-level dynamic pressure.

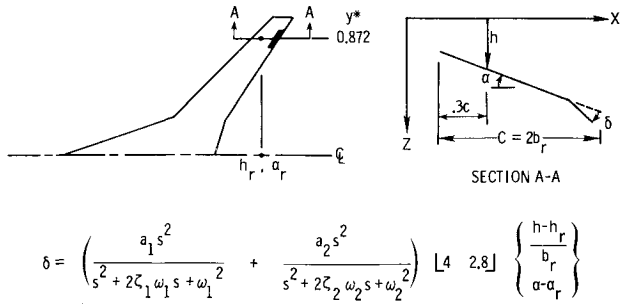

Fig. 8 General scheme for aerodynamic energy method.

$\lfloor G \rfloor = \lfloor 4 \quad 2.8 \rfloor$

$[\phi]$ = matrix of the difference of modal coefficients at sensor locations

that is,

$$\begin{Bmatrix} \dfrac{h-h_r}{b_r} \\ \alpha-\alpha_r \end{Bmatrix} = [\phi]\{q\}$$

The matrix $\lfloor G \rfloor$, derived in the relaxed energy method,[8] indicates the relationship between bending displacement and angle of attack which provides feedback to the control surface and is fixed for all applications using a 20% chord control.

The synthesis procedure is to determine those values of the free parameters a_1, a_2, ζ_1, ζ_2, ω_1, and ω_2, Eq. 9, which provide, over a wide range of operating conditions, the required stability margin with minimum control surface activity in a gust environment. This determination is accomplished by first assigning values to the free parameters which stabilize the system to the required velocity margin. Experience has shown that if the free parameters are changed in a way to reduce the stability of the system, the control surface activity in a gust environment increases. Hence, the free parameters can be determined by minimizing the response of the system to a gust input. In this manner, the gust becomes a driver in establishing the closed-loop free parameters while maintaining stability. This procedure can be described in the following steps:

1) Assign initial values to the free parameters which stabilize the system at the desired Mach number and dynamic pressure.

2) With values of the free parameters determined in step 1, determine new values of the free parameters which result in minimum control surface activity (rates or displacements) in a continuous gust analysis. The algorithm used for minimization is a variation of the Steward adaptation[12] of the Davidon Fletcher Powell method.[13]

3) Perform a sensitivity study by varying each of the free parameters at a number of design points to establish a system that will perform satisfactorily over a wide range of flight conditions.

4) Check system stability using a root locus calculation.

If, after this process is completed, the required control surface activity is unacceptable; then either the control surface must be increased in size or more control surfaces must be added and the process repeated.

Closed-Loop Control Law

For purposes of comparison, the control surface location is the same as that for the classical approach described earlier. As a general rule, the control surface should be placed in an area of maximum modal displacement in the flutter mode and, in fact, this requirement is met here.

The control surface has a 20% chord, and the wing sensor is placed in the center of the spanwise wing strip, defined by the edges of the control surface, at the 30% chord point (see Fig. 8). Although not indicated, angle of attack of the strip is determined by differencing two accelerometers located at the 30% and 70% chord points, respectively.

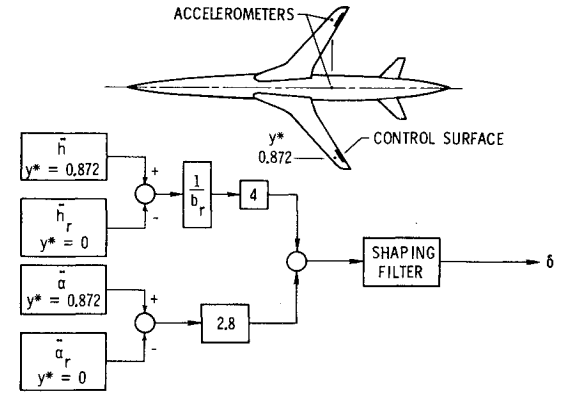

Fig. 9 Synthesized active control system – aerodynamic energy method.

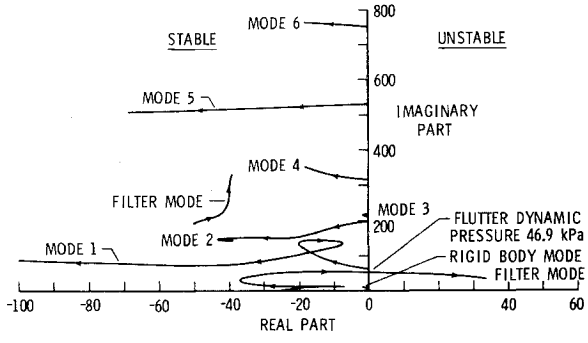

Fig. 10 Closed-loop root locus at $M=0.9$ and altitude = 1676 m (aerodynamic energy method).

Step 1 of the procedure is achieved by using the following values for the free parameters in Eq. (9).

$$a_1 = 3.0 \qquad \omega_1 = 80 \qquad \zeta_1 = 0.5$$
$$a_2 = 3.0 \qquad \omega_2 = 120 \qquad \zeta_2 = 0.5$$

The values of ω_1 and ω_2 band the basic wing flutter frequency. Initial estimates for a_1 and a_2 both equal to 2 had to be increased in order to meet stability requirements.

Step 2 of the procedure was achieved by varying the values of the free parameters over the following ranges:

$$0 \le (a_1, a_2) \le 3.5$$

$$0.25 \le (\zeta_1, \zeta_2) \le 1.0$$

$$25 \le (\omega_1, \omega_2) \le 200$$

Control surface rates appeared to dominate the design, so the minimization algorithm was used at the maximum flight dynamic pressures at $M=0.7$, 0.8, and 0.9 to determine free parameter values that minimize control surface rates at each of these selected conditions. The difficulties with a point design became apparent when each of these control laws was then tested at other flight conditions. That is, control surface rates were minimized at each of the selected conditions, but this process did not guarantee satisfactory operation at other flight conditions. Step 3 was then carried out by performing sensitivity studies at the maximum dynamic pressures at $M=0.7$ and 0.9. The free parameters were varied over a range of values at these two selected conditions to determine a suboptimal control law that would minimize control surface

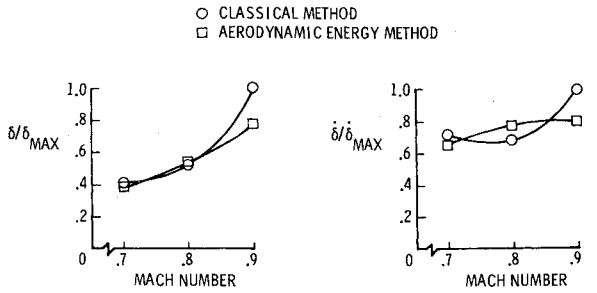

Fig. 11 Comparison of control surface rates and displacements.

activity over the range of design conditions. Step 4 was then performed at $M=0.7$, 0.8, and 0.9 to insure that system stability was achieved. As a result of this procedure, the following form of the control law was developed:

$$\delta(s) = \left(\frac{3s^2}{s^2 + 2(1)25s + (25)^2} + \frac{1.6s^2}{s^2 + 2(.25)200s + (200)^2} \right) \times \lfloor 4 \;\; 2.8 \rfloor [\phi]\{q\}$$

A plan view of the vehicle indicating control surface locations, sensor locations, and a simplified block diagram of the closed loop system is presented in Fig. 9.

System Performance

A typical closed-loop root locus at $M=0.9$ and altitude = 1676 m is shown in Fig. 10. Comparing these results with the no-control case, Fig. 3, indicates an increase in flutter dynamic pressure of approximately 95%. The method by which the flutter is delayed appears to be similar to that for the classical method, Fig. 7; however, the closed-loop flutter point occurs at a dynamic pressure of 46.9 kPa for this case. The closed-loop results at $M=0.9$, 0.8, and 0.7 are presented in Table 1.

Discussion

Both synthesis methods result in closed-loop systems that achieve the required objectives, i.e., a 20% increase in the flutter velocity with control rates and deflections that are achievable in a realistic gust environment. These objectives are met throughout the operating envelope that was analyzed.

Two major differences result in the application of these methods. The first difference is in establishing the form, gains, and break frequencies of the shaping filter. In the classical method, this process is a function of previous experience coupled with the results of analysis for the particular system being studied and, in general, cannot be extended to other problems. In the aerodynamic energy method, on the other hand, a fixed form of the shaping filter is given with free parameters available to fit this form to the dynamic characteristics of the system being considered.

The second difference is the manner in which the gust analysis is used. In the classical method the gust is used to evaluate rates and deflections of the control system after preliminary design of the shaping filter is complete. If the rates or deflections are beyond the capability of the control system, then an iterative process including changes to the shaping filter and possibly the control surface size is begun. This process is continued until both the stability and gust response requirements are met. In the energy method, the fixed form of the shaping filter allows the gust to act as a driver in establishing the free parameters, which in turn permits the minimization of control surface activity while maintaining stability.

As a comparison of the control surface activity for the two methods, Fig. 11 presents ratios of the control surface rates and displacements. Results from both methods are ratioed to the maximum value for the classical method. For the Mach numbers investigated, this maximum occurs at $M=0.9$, altitude = 3050 m. Reductions in both maximum rates and displacements on the order of 20% are evident. In addition (Table 1), at $M=0.9$, the closed-loop flutter dynamic pressure is approximately 8% higher for the energy method.

Concluding Remarks

Two preliminary synthesis studies of an active flutter suppression system, which permit flight testing of a research wing at speeds up to 20% above the basic wing flutter boundary, are described. The first study uses classical control theory, while the second uses an "aerodynamic energy method" to formulate control laws. While both synthesized systems are capable of providing the required flutter margin, over a wide range of altitude and subsonic Mach number, it is shown that the energy method can be used in conjunction with optimization procedures to minimize control surface activity while maintaining system stability.

Acknowledgment

The authors acknowledge the work of E. Nissim of the Technion, Haifa, Israel, in his original development of the aerodynamic energy method and recent advances in this area. Many of the analysis procedures reported here were developed by Nissim while he was a National Research Council Senior Postdoctoral Associate at the NASA Langley Research Center.

References

[1] "Advanced Control Technology and Its Potential for Future Transport Aircraft," NASA TM X-3409, 1976.

[2] Schoenman, R.L. and Shomber, H.A., "Impact of Active Controls on Future Transport Design, Performance, and Operation," SAE Paper 75-1051, National Aerospace Engineering and Manufacturing Meeting, Culver City, Nov. 1975.

[3] Doggett, R.V. and Townsend, J.L., "Flutter Suppression by Active Controls and Its Benefits," *Proceedings of the SCAR Conference,* NASA CP-001, 1976.

[4] Sanford, M.C., Abel, I., and Gray, D.L., "Development and Demonstration of a Flutter Suppression System Using Active Controls," NASA TR R-450, 1975.

[5] Nissim, E., "Flutter Suppression Using Active Controls Based on the Concept of Aerodynamic Energy," NASA TN D-6199, 1971.

[6] Redd, L.T., Gilman, J., Cooley, D.E., and Sevart, F.D., "A Wind-Tunnel Investigation of a B-52 Model Flutter Suppression System," AIAA Paper 74-401, Las Vegas, Nev., April 1974; also *Journal of Aircraft,* Vol. 11, Nov. 1974, pp. 659-663.

[7] Visor, O.E. and Sevart, F.D., "Preliminary Design Study of Flutter Suppression Control System for BQM-34E/F Drone Aircraft with a Supercritical Wing – Final Report," NASA CR-145208, 1976.

[8] Nissim, E., "Application of the Aerodynamic Energy Concept to the Selection of Transfer Functions for Flutter Suppression and Gust Alleviation Using Active Controls," AIAA Paper 77-423, San Diego, Calif., March 1977.

[9] Nissim, E., Caspi, A., and Lottati, I., "Application of the Aerodynamic Energy Concept to Flutter Suppression and Gust Alleviation by Use of Active Controls," NASA TN D-8212, 1976.

[10] Albano, E. and Rodden, W.P., "A Doublet-Lattice Method for Calculating Lift Distributions on Oscillating Surfaces in Subsonic Flows," *AIAA Journal,* Vol. 7, Feb. 1969, pp. 279-285.

[11] Sevart, F.D., "Development of Active Flutter Suppression Wind Tunnel Testing Technology," AFFDL-TR-74-126, 1975.

[12] Stewart, G.W., "A Modification of Davidon's Minimization Method to Accept Difference Approximations of Derivatives," *Journal of the Association for Computing Machinery,* Vol. 14, Jan. 1967, pp. 72-83.

[13] Fletcher, R. and Powell, M.J.D., "A Rapidly Convergent Descent Method for Minimization," *Computer Journal,* Vol. 6, July 1963, pp. 163-168.